Proceedings of the General Donald R. Keith Memorial Conference
of the Society for Industrial and Systems Engineering,
West Point, New York, USA
April 30, 2015

Decision Support Tool for Designing Niche Small Package Delivery Aerial Vehicles (DST-NSPDAV)

Ashruf Ali, Nathan Ballou, Brad McDougall, and Jorge Luis Valle

George Mason University

Department of Systems Engineering and Operations Research

Email: aali21@gmu.edu , nballou@gmu.edu , bmcdoug2@gmu.edu , jvallera@gmu.edu

Author Note: The authors of this paper are senior systems engineering students from George Mason University's Systems Engineering and Operations Research Department that are concluding their senior capstone design projects.

Abstract: A growing market is the application of multi-rotor vehicles to niche delivery services such as just-in-time spare parts delivery, real-time asset repositioning, rapid food delivery, and remote medical supply delivery. These services are unique in their requirements, meaning there is no single aerial vehicle configuration that is optimal for every scenario. More importantly, these service providers do not have the expertise to design and operate small multi-rotor vehicles that are now feasible due to advances in technology. This is a complex design decision with non-linearities in the design-state-space. This paper presents a decision-support tool to assist small package delivery service providers on choosing the best multi-rotor vehicle for their payload application.

The decision-support tool for the design of multi-rotor small package delivery aerial vehicles (SPDAV) takes inputs such as payload range, minimum distance, maximum price and size, and recommends suitable pre-existing configurations. A configuration is defined as a frame size and weight, number of rotors and rotor torque, battery (size, voltage, amperage), propeller, and micro-controller. The algorithm used to generate the design-state-space consists of two separate models of multi-rotor aircraft: (1) a power consumption model and (2) a full dynamic flight model. The power consumption model evaluates the steady-state performance of the battery, motor, and propeller combinations at hover, 80%, and full throttle to determine systems that satisfy the users' requirements. A dynamic flight model is then applied to these pre-existing configurations to further account for airframe aerodynamics.

Keywords: Power-Model, Dynamic-Model, Multi-Rotor

1. Context

1.1 Multi-Rotor Aerial Vehicles

Modern day advances in batteries, microcontrollers, and lightweight materials have led the unmanned multi-rotor aerial vehicle market away from being merely hobbyists toys to now mass produced aircraft with commercial applications. Multi-rotors, for the sake of this paper, are rotorcraft with more than two propellers that do not have varying pitch and are capable of vertical takeoff and landing. This allows for easier flight control because movement is achieved by simply deviating the power to propellers, making programmable flight control a viable capability. The reliability and maintainability is also superior to traditional rotorcraft due to the simpler rotor mechanics from less required moving parts. Multi-rotors are relatively small, with size ranging from one to ten feet tip-to-tip, making them more responsive and easier to change direction. Most importantly, multi-rotors are commercially off the shelf available with a wide variety in custom and pre-built configurations. A multi-rotor configuration is defined by the authors as a frame size and weight, number of rotors and rotor torque, battery (size, voltage, amperage), propeller, and micro-controller.

1.2 Small Package Delivery

Large companies such as Amazon, Google, DHL, and Dominos have recognized the capability of the multi-rotor aerial vehicles and have invested in straightforward package delivery. With their financial and intellectual resources, these companies are positioned to leverage this technology. In addition to package delivery, there exist many other *niche* delivery services such as just-in-time spare parts delivery, real-time asset repositioning, rapid food delivery, and remote medical supply delivery. These services are unique in their requirements, meaning there is no single aerial vehicle configuration that

is optimal for every application. More importantly, these service providers do not have the in-house expertise or financial resources to design and operate small multi-rotor vehicles.

1.3 Design-Engineering Difficulties

Despite being relatively simple in design when compared to other aerial vehicles, the challenge for designing multi-rotors is due to the large amount of possible configurations and the non-linear interactions in the design-space. Choosing a configuration that meets a set of requirements optimally is not possible without expertise or a decision-support tool.

One of the difficulties incurred during the design of multi-rotors is the non-linearity in the trade-space. For instance, a change to the battery does not mean one can expect some incremental correlated change to the distance capable of being traveled. For example, while evaluating the total payload, one must ensure there is enough power to handle the increased weight. This will then require a battery that is capable of keeping up with the increased need for power. In order to support this larger battery, an adequate frame will be needed. With this now overall increase in total weight one will need more power, and the cycle continues.

1.4 Problem Statement

The advances in multi-rotor aerial vehicle technologies have enabled applications for small package delivery. Unlike the large logistics companies with financial and intellectual resources to design and operate these vehicles from a complex and non-linear design-space, enterprises with niche applications (e.g. asset repositioning, spare parts delivery, rapid food or flower delivery) do not have the expertise to design the optimum vehicle to meet the requirements of their application.

2. Method of Analysis

2.1 Decision-Support Tool Overview

The DST is conducted in two stages – first a power model to identify promising multi-rotor configurations and then a full dynamic model to further characterize the specific performance of these pre-existing configurations.

For the power model, the user defines the distance to travel, payload range, and maximum price and size. These factors are then put through a simulation to approximate the power draw, motor temperature, hover characteristics, and flight duration under normal loads. This portion of the simulation is fed with currently manufactured multi-rotor configurations. Unreasonable configurations (hovering requires greater than 80% throttle, maximum cost or size exceeded, motor temperature at maximum throttle exceeding 80 degrees Celsius) are removed from further analysis.

The full dynamic model takes these viable configurations and subjects them to a more detailed simulation. The model simulates the multi-rotor's performance over a default flight path. Maximum flight distance for a given configuration is found by running the simulation multiple times and applying Newton's method to determine the distance corresponding to a battery drain from 80% to 10% to account for battery degradation and provide a cushion of performance safety. The simulation is conducted for a low wind environment which is assumed to be 0 mph and package weights corresponding to user inputs. Figure 1 below outlines the entire functionality of the DST.

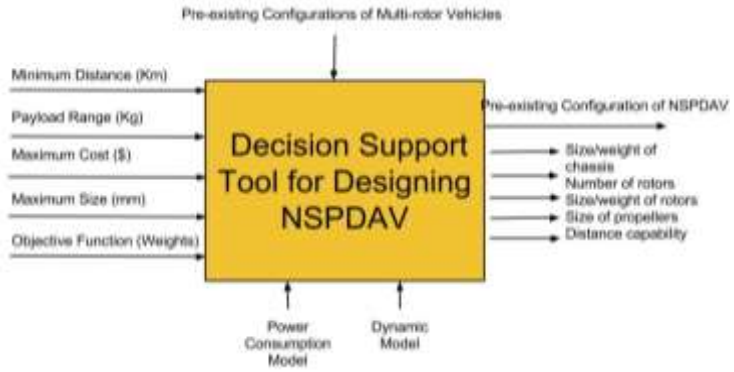

Figure 1. DST Functionality

2.2 Dynamic Model Coordinate System

The dynamic simulation is a more detailed simulation for highly ranked outputs of the preliminary simulation steps. The simulation models frame aerodynamics; propeller thrust; motor, electronic speed controller, and battery system performance; and inertial response to output a detailed picture of the multi-rotor's performance. This information is used to approximate the flight characteristics of the multi-rotor over a default flight profile, and payload range.

The dynamic simulation operates in a six degree of freedom environment. The position of the body in space is both defined by translational motion in the x-y-z axis and by Euler angles $\psi - \theta - \phi$, referred to as yaw, pitch, and roll. The simulation defines three coordinate systems in this 6-DoF environment: an inertial North East Down (NED), a body frame, and a geodetic. The inertial frame is fixed on the starting location of the simulated flight profile, and defines the location and orientation in relative space. The body frame is fixed on the multi-rotor's center of gravity. This origin decouples actuation forces and moments and allows for a constant moment of inertia tensor. The locations and orientations of the body and inertial frame are as shown below in Figure 2.

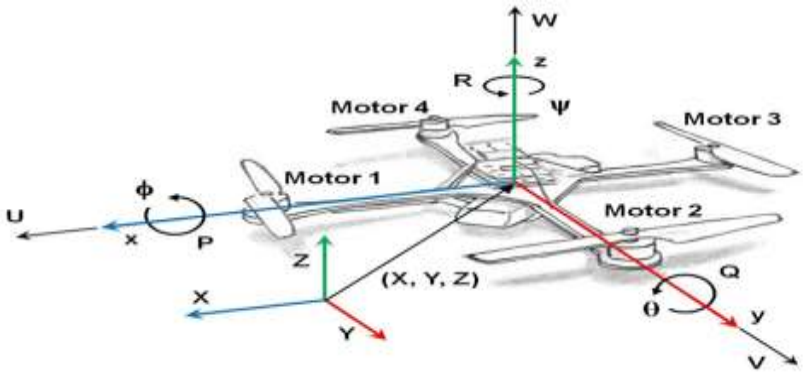

Figure 2. Body and Inertial Frame

Transformation maticies are used to represent translation and rotation in both coordinate systems. Motion in the body frame is transformed through $\psi - \theta - \phi$ rotations as shown in (1). Combining these transformations yeilds the direction cosine matrix H_B^I displayed in (2). For example, velocity measured in the body frame is transformed to the inertial frame as $v_I = H_B^I v_b$. A similar transformation (3) is performed for angular velocities and accelerations where p, q and r are rotational velocities around each translational axis (4). It should be noted that this transformation matrix yields singular results around $\theta = \frac{\pi}{2}$. We deem this limitation acceptable as small package delivery does not typically encounter such aggressive flight maneuvers. Should such maneuvers be desired, a switch to a quaternion representation could be implemented.

$$\mathrm{H_I^1}(\psi) = \begin{bmatrix} \cos\psi & \sin\psi & 0 \\ -\sin\psi & \cos\psi & 0 \\ 0 & 0 & 1 \end{bmatrix}, \mathrm{H_1^2}(\theta) = \begin{bmatrix} \cos\theta & 0 & -\sin\theta \\ 0 & 1 & 0 \\ \sin\theta & 0 & \cos\theta \end{bmatrix}, \mathrm{H_2^B}(\phi) = \begin{bmatrix} 1 & 0 & 0 \\ 0 & \cos\phi & \sin\phi \\ 0 & -\sin\phi & \cos\phi \end{bmatrix} \quad (1)$$

$$\mathrm{H_B^I}(\phi, \theta, \psi) = H_I^1 \mathrm{H_1^2 H_2^B} = \begin{bmatrix} \cos\theta\sin\psi & \sin\phi\sin\theta\cos\psi - sin\psi cos\phi & \cos\phi\sin\theta\cos\psi + \sin\phi\sin\psi \\ \cos\theta\sin\psi & \sin\phi\sin\theta\sin\psi + \cos\phi\cos\psi & \cos\phi\sin\theta\cos\psi - \sin\phi\sin\psi \\ -\sin\theta & \sin\phi\cos\theta & \cos\phi\cos\theta \end{bmatrix} \quad (2)$$

$$\begin{bmatrix} \mathrm{p} \\ \mathrm{q} \\ \mathrm{r} \end{bmatrix} = \mathrm{I_{3x3}} \begin{bmatrix} \dot{\phi} \\ 0 \\ 0 \end{bmatrix} + \mathrm{H_2^B} \begin{bmatrix} 0 \\ \dot{\theta} \\ 0 \end{bmatrix} + \mathrm{H_2^B H_1^2} \begin{bmatrix} 0 \\ 0 \\ \dot{\psi} \end{bmatrix} \quad , \quad \mathrm{L_B^I}(\phi, \theta, \psi) = \begin{bmatrix} 1 & \sin\phi\tan\theta & \cos\phi\tan\theta \\ 0 & \cos\phi & -\sin\phi \\ 0 & \sin\phi/\cos\theta & \cos\phi/\cos\theta \end{bmatrix} \quad (3,4)$$

Finally, a geodetic axis is used to more accurately approximate local gravity conditions. Transformations are approximated using the WGS84 standard using the following formula (5).

$$x = (N + h)\cos\phi'\cos\lambda', y = (N + h)\cos\phi'\sin\lambda', z = \left(\left(\frac{b^2}{a^2}\right)N + h\right)\sin\phi', \text{where } N = \frac{a}{\sqrt{1-e^2\,sin^2\,\phi}} \quad (5)$$

2.3 Models and Theories Utilized

The dynamic model consists of the following self-contained modules:

2.3.1 Body Geometric and Inertial Calculations

The dynamic simulation begins with the definition of the current vehicle simulation. This definition includes mass, dimensions, and performance properties of the motors, central hub, arms, payload, and propellers. These components are modeled as simple solids to approximate the overall mass, moments of inertia, and geometric conditions. Motors and the central hub are modeled as cylinders and the arms and payload as cuboids. Propellers are represented as thin rectangles for the purpose of these approximations.

The first characteristic of the model approximated is the overall vehicle mass. This is simply the sum of the individual components. This sum is then used to define the center of mass for the representative model. For the purposes of this simulation, the multi-rotor vehicles are assumed to be symmetrical in the vertical and horizontal planes. The following defines the distance from the center of the central cylinder to the center of gravity on the z-axis (6). All component locations are then redefined on the new body origin at this location.

The simple solids model is then used to calculate the overall inertial moments for the vehicle. This involves first calculating the moment of inertia for each individual component, transforming it to be parallel to the main body axis (7) (8), and then using the parallel axis theorem to form the complete moment value (9).

This solids approximation is also used to estimate the surface area for use in drag calculations. For a quadcopter example, the following is the projected side and vertical surface area (10). Lastly, the approximate centroid is calculated (11) to define the point of drag action using the corner points of the approximated multi-rotor shape.

$$G = \frac{n_r\left[m_m\left(\frac{z_a}{2}+\frac{z_m}{2}\right)+m_p\left(\frac{z_a}{2}+z_m+z_s\right)\right]-m_p\left(\frac{z_c}{2}+\frac{z_p}{2}\right)}{m_{tot}} \quad (6)$$

$$I_L = TI_{LR}T^T,\ T = \begin{bmatrix}\cos\theta & \sin\theta & 0\\ -\sin\theta & \cos\theta & 0\\ 0 & 0 & 1\end{bmatrix}, \qquad I_O = I_L + md^2 \quad (7,8,9)$$

$$A_X = A_Y = 2r_ch_c + 2l_ah_a + 4r_mh_m + l_ph_p \quad A_Z = w_pl_p + 4l_aw_a + 4\pi r_m^2 \ , \ C = \frac{1}{k}\sum_i^k x_i \quad (10,11)$$

2.3.3 Motor Model

The motor model approximates the performance of a brushless dc (BLDC) electric motor. These motors were chosen for their high power to weight ratios, efficiency, and low maintenance requirements and are standard components in current multi-rotor UAVs. The model is based on Kirchhoff's voltage law (13) and Newton's second law (14) as described by Movellan (2010) with some alterations.

The inductance of the motor is very difficult to measure and is, in any case, very small for this type of motor, so it will be neglected (15). The load torque has quadratic dependence on motor and propeller angular velocity, so $\tau_{load} = d\Omega^2$ (16).

The BLDC motors used in this application reach steady state very quickly due to low inductance and rotational inertia. The time constant for no load is approximately 0.03 s, significantly smaller than the simulation step time. The model is therefore further simplified to assume steady state operation (17). Rearranging shows the voltage required to reach a desired motor speed (18).

$$V = L\frac{dI}{dt} + RI + K\Omega \quad , \quad J\frac{d\Omega}{dt} = KI - \lambda\Omega - \tau_{load} \quad (13,14)$$

$$V = RI + K\Omega \quad , \quad J\dot{\Omega} = -\frac{K^2}{R}\Omega - d\Omega^2 + \frac{K}{R}V \quad (15,16)$$

$$\Omega^2 + \frac{K^2}{Rd}\Omega - \frac{K}{Rd}V = 0 \quad , \quad V = \frac{Rd}{K}\Omega^2 + K\Omega \quad (17,18)$$

2.3.4 Aerodynamic Model

The aerodynamic model uses the projected surface area calculated before as described by Moyano (2013) to calculate the airframe drag. The general form of the drag equation (19) is modified for this purpose as below. This general form is first modified to take into account the varying surface area and drag coefficient based on relative orientation (20). We can therefore calculate the individual components of the drag as follows (24).

The area function is approximated based on the sideslip and angle of attack of the vehicle. This simplification is used due to the relatively crude geometric representation and computational difficulties of estimating instantaneous frontal surface area. We therefore approximate the area as a ratio of the frontal and side areas (22).

The C_d value is much more difficult to approximate. An accurate calculation would involve a CFD analysis on a specific frame geometry and propeller wake properties - an analysis far beyond the scope of this simulation. We therefore estimate the drag coefficient as a function between a max and min C_d value based on experimental data.

Lastly, the relative centroid based on airflow direction must be calculated to complete the aerodynamic force characterization. The drag moment is approximated in a manner similar to the frontal surface area (23)(24).

$$F_d = \frac{1}{2} C_d \rho A v^2 \quad , \quad F_d = \frac{1}{2} \rho C_d(\beta_{SS}, \alpha) A(\beta_{SS}, \alpha) V_\infty^2 \quad , \quad F_d = \begin{cases} F_{dx} = F_d \cos\beta_{SS} \cos\alpha \\ F_{dy} = F_d \sin\beta_{ss} \cos\alpha \\ F_{dz} = F_d \sin\alpha \end{cases} \qquad (19,20,21)$$

$$A \cong A_x \cos\beta_{SS} \cos\alpha + A_y \sin\beta_{SS} \cos\alpha + A_z \sin\alpha \qquad (22)$$

$$M_d = r_d(\beta_{ss}, \alpha) \times F_d \quad M_d = r_d(\beta_{SS}, \alpha) \sin\theta_d F_d \quad , \quad r_d \cong r_{dx} \cos\beta_{SS} \cos\alpha + r_{dy} \sin\beta_{SS} \cos\alpha + r_{dz} \sin\alpha \qquad (23,24)$$

The simplifications above may result in significant deviations from experimental data collected in the validation stage. Further work may be needed to more accurately approximate this phenomenon.

2.4 Utility Model

The utility model takes into account utility weights obtained by using the swing weights method. It accounts for the average distance, average speed, and the multi-rotor size. It also takes into account the Mean Time between Failure (MTBF), which is associated with the reliability of motors, and batteries. Below is the equation used to calculate the utility for all pre-existing configuration:

$$Utility = w1 * (Average\ Distance) + w2 * (Average\ Speed) + w3 * (Size) + w4 * (MTBF) \qquad (25)$$

3. Case Study: GMU Fast Food Restaurant

The requirements for the case study are as follows: payload range between 1.0 Kg and 4.0 Kg, minimum distance of 2.0 km (4.0 km round trip), maximum cost of $20,000, and maximum width of 1700 mm (from tip to tip). Furthermore, a survey is completed in which utility weights are calculated using the swing weights method.

The assumptions taken into account are that the multi-rotor will operate autonomously, have easy customer destination input, and be monitored from the ground. The flight path will maintain a safe environment for the population within the area of operation by avoiding flight over traditional routes taken and instead flying over areas uninhabited or lightly traveled upon. In order to meet these requirements, the simulation evaluated the following pre-existing multi-rotors shown in Table 1:

Table 1. Multi-Rotor Configurations from DST Database

	Rotors	Total Weight (g)	Battery (mAh)	Propellers	Motor (Kv)	Width (mm)	MTBF (hours)	Cost
DJI-S800	6	4400	15000 (4S)	15x4" APC	415	1180	100	
FAE-960H	6	9500	16000 (4S)x2	18x6" APC	480	1420	160	$9,988
X8-HLM	8	3250	10000 (4S)	10x4.7" APC	880	1350	150	
OFM-GQ8	8	6500	16000 (6S)	17x5.8" APC	420	1530	160	$10,299
HL48	8	7800	16000 (6S)	15x4" APC	520	1450	160	$15,000

After running the simulation, only three of the five multirotor aircrafts shown above are able to work with a payload up to 4 kg due to their battery capacity, propeller size and motor properties. The average of the distance and speed for the remaining three multi-rotor configurations, shown in Table 2, are calculated in order to be normalized alongside the size and the mean time between failures (MTBF) of each configuration. These values are used to calculate the final utility score, shown in Table 3, by multypling them with the weights for each parameter:

Table 2. Averages for 1-4kg Payload

Model	Average Distance (Km)	Average Speed (Km/h)
FAE-960H	3.8	30.3
OFM-GQ8	3.7	42.8
HL48	2.5	38.3

Table 3. Utility Scores

	Distance	Speed	Size	MTBF	
Weights	**0.365**	**0.365**	**0.090**	**0.180**	**Utility Score**
FAE-960H	0.95	0.67	0.16	1.00	0.7857
OFM-GQ8	0.93	0.95	0.10	1.00	0.8752
HL48	0.63	0.85	0.15	1.00	0.7337

The final recommendation for this case study is to work with the OFM-GQ8 octocopter. This configuration covers the distance required from the end user, works with the payload given, and flies faster than the other evaluated configurations.

It is worth noticing that the best utility value is not related to the most expensive multirotor aircraft and this is due to many different factors such as the size of the propellers, the weight of the aircraft, or the rate of battery drain. It is also important to note that different end users will present different requirements and a market evaluation is necessary in order to assure that multi-rotors are a viable and profitable solution to their niche small package delivery application.

5. References

Banura, M & Mahony, R. (2012, December). Nonlinear Dynamic Modeling for High Performance Control of a Quadcopter.
Bresciani. T. (2008). Modeling, Identification and Control of a Quadrotor Helicopter.
Capello, E. (2012, October). Mini Quadrotor UAV: Design and Experiment.
Fresk, E. (2006, July). Full Quaternion Based Attitude Control for a Quadrotor.
Hartman D., Landis, K., Mehrer, M., Moreno, S., & Kim, J. (2014, July) Quadcopter Dynamic Modeling and Simulation.
Kim, J. (2009, September). Accurate Modeling and Robust Hover Control for a Quad-rotor VTOL Aircraft.
Latorre, E. (2011, June). Propulsion System Optimization for an Unmanned Lightweight Quadrotor.
Leishman, J.G.. (2002). Principles of Helicopter Aerodynamics 2nd Edition.
Mansson, C. (2014, June). Model-based Design Development and Control of a Wind Resistant Multirotor UAV.
Martinez, V. (2007, September). Modeling of the Flight Dynamics of a Quadrotor Helicopter.
Movellan, J.R..(2010). DC Motors, Machine Perception Laboratory, University of California.
Moyano, J. (2013). Quadrotor UAV for wind profile characterization.
NIMA. (2000, January) Department of Defense World Geodetic System 1984.
Pounds, P. (2006, December). Modelling and Control of a Quad-rotor Robot.
Prouty, R.W. (1990). Helicopter Performance, Stability and Control.